

# Orbit-Attitude Coupled Dynamics of Solar Sail Spacecraft around Small Bodies

By Shota KIKUCHI,<sup>1)</sup> Yuichi TSUDA,<sup>2)</sup> and Jun'ichiro KAWAGUCHI<sup>2)</sup>

<sup>1)</sup>*Department of Aeronautics and Astronautics, The University of Tokyo, Tokyo, Japan*

<sup>2)</sup>*Institute of Space and Astronautical Science, JAXA, Sagamiara, Japan*

Rendezvous missions to small bodies, such as asteroids and comets, have been of interest in recent years. The motion of a spacecraft in the proximity of a small body is significantly perturbed primarily due to the irregular shape of the small body and solar radiation pressure. In such a strongly perturbed environment, the coupling effect of the orbital and attitude motion has a significant effect that cannot be neglected. In addition, when the exposed surface of a spacecraft is deformed, the effect of solar radiation pressure completely differs from that of a spacecraft that has an ideal flat surface. In particular, this deformation effect is dominant for a solar sail spacecraft having a huge and flexible membrane. However, natural orbit-attitude coupled dynamics of solar sail spacecraft around small bodies that are stationary in both the orbital and attitude motions have yet to be observed. The present study therefore investigates the natural coupled motion of solar sail spacecraft that involves both a Sun-synchronous orbit and a Sun-tracking attitude motion. This orbit-attitude coupled motion enables a spacecraft to maintain its orbital geometry and attitude state with respect to the Sun without requiring active control. Thus, the proposed method can reduce the use of orbit and attitude control systems, which reduces the weight of a spacecraft and prolongs the life time of the mission. The present study investigates the theory behind achieving Sun-synchronous orbits with Sun-tracking attitude motion for a solar sail spacecraft. Moreover, several simulations are performed, assuming a Jovian Trojan asteroid exploration mission with solar sail spacecraft (which is scheduled to be launched by JAXA in the early 2020s). It is thereby demonstrated that this novel orbit-attitude coupled motion is feasible and useful for small-body missions.

**Key Words:** Small body, Solar sail, Sun-synchronous orbit, Sun-tracking motion, Orbit-attitude coupled motion

## 1. Introduction

Small celestial bodies, such as asteroids and comets, often retain information on the dynamical evolution of the solar system. Thus, rendezvous missions to small bodies play a key role in understanding our solar system. In such missions, a spacecraft faces unique difficulties from the perspective of dynamics around the target body. First, the gravity of a small body is very weak, and therefore, the motion of a spacecraft is perturbed by the solar radiation pressure (SRP). In addition, irregular gravitational field around a small body also perturbs the motion of a spacecraft. Because of these perturbations, the dynamics of spacecraft around small bodies is complex and completely differs from that around planets.

This intriguing environment around small bodies has been investigated in many previous studies for both orbital and attitude dynamics. The orbital motion subject to SRP perturbation and gravity irregularity exhibits significant changes in orbital elements.<sup>1)</sup> One of the proposed solutions to this problem is implementing Sun-synchronous frozen orbits, for which the orbital geometries are constant with respect to the Sun, as depicted in Fig. 1(a).<sup>2-5)</sup> On the other hand, the attitude dynamics around small bodies is unique in that it can be predominantly affected by gravity gradient (GG) torque due to the higher order gravitational terms.<sup>6,7)</sup> It has been revealed that the stability behavior of the attitude motion is dependent on the shape of a small body.<sup>8,9)</sup> In addition to the GG torque, the SRP torque can also exert an influence on the attitude of a spacecraft, resulting in more complex dynamics.<sup>10)</sup>

Although the studies described above analyze the orbital motion and the attitude motion of a spacecraft separately, these motions are not independent in reality. For example, GG torque

varies depending on the position of a spacecraft about a gravitational mass; at the same time, the gravitational force and the SRP force are dependent on the attitude state when the spacecraft is modeled as a rigid body.<sup>12)</sup> Recent studies have discovered that such orbit-attitude coupling effect significantly impacts the motion of a spacecraft under the strongly perturbed environment in the vicinity of a small body.<sup>13-15)</sup> These dynamical features around small bodies lead to the frequent use of orbit and attitude control systems, such as thrusters and reaction wheels.

To circumvent this problem, the authors have recently identified the natural orbit-attitude coupled motion that involves both a Sun-synchronous orbit and a Sun-tracking attitude motion, as illustrated in Fig. 1.<sup>11)</sup> The proposed method enables a spacecraft to maintain its orbital geometry and attitude state with respect to the Sun without requiring any active control. For this

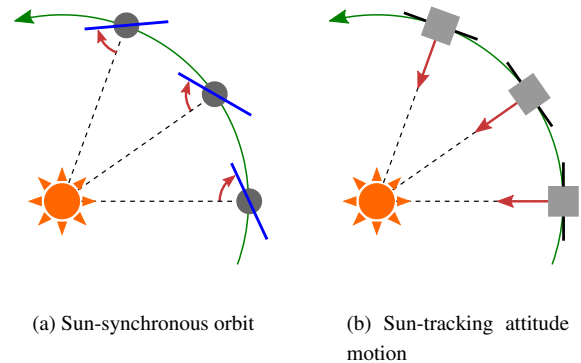


Fig. 1. Sun-synchronous orbit and Sun-tracking attitude motion.<sup>11)</sup>

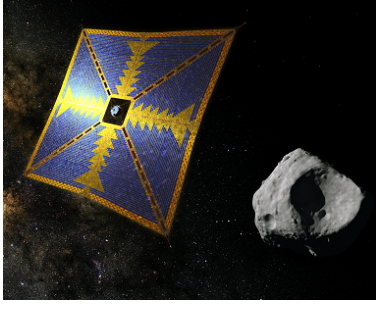


Fig. 2. JAXA's solar power sail for the Trojan asteroid mission.<sup>18)</sup>

reason, the implementation of a Sun-synchronous orbit with a Sun-tracking attitude motion is advantageous for solar power generation, thermal design, and optical observation. Besides, it can reduce the use of the orbit and attitude control systems, thereby reducing the mass of a spacecraft, prolonging the life time of the mission, and reducing the operational workload.

In particular, this type of orbit-attitude coupled motion offers a major advantage to a solar sail spacecraft having a huge membrane, because conventional reaction control systems require large resources for a spacecraft with a large moment of inertia. The authors' previous research on the coupled orbit-attitude dynamics around small bodies was designed for a spacecraft with an ideal flat surface.<sup>11)</sup> However, when the membrane of a solar sail spacecraft is deformed, the effect of SRP differs from that of a spacecraft that has an ideal flat surface.<sup>16)</sup> Therefore, this study extends the theories in our previous paper by taking into account the deformation of the surface exposed to the solar radiation. The extended theories are also applicable for a spacecraft mounting solar array paddles with gimbal mechanism that cannot be modeled as a single flat plate. The novel dynamics presented in this paper exhibits unique and variable characteristics.

The present study was designed to develop general theories of coupled orbit-attitude motion of solar sail spacecraft around small bodies. First, the orbital motion is modeled as Lagrange planetary equations, and the solutions of Sun-synchronous orbits are analytically solved. Next, the attitude motion is modeled as linearized Euler equations, and conditions required to achieve Sun-tracking motion are derived. The analyses of attitude motion consider the SRP effect of non-flat surfaces that is not taken into account in our previous research. Last, the orbital and attitude motions are propagated by numerical integration on the basis of non-linear equations of motion including the orbit-attitude coupling effect. The analytical and numerical analyses are performed for the Jovian Trojan asteroid exploration mission with a solar power sail, which is scheduled to be launched by JAXA in the early 2020s.<sup>17,18)</sup> It is thereby demonstrated that the proposed method is feasible for real missions.

## 2. Dynamics model

### 2.1. Spacecraft and small body model

The physical parameters for a spacecraft used in this paper are given in Table 1. These parameters are based on JAXA's solar power sail for the Trojan asteroid mission. Throughout this paper, the  $z$  axis of the spacecraft body-fixed frame is regarded as the axis that should be directed toward the direction

Table 1. Spacecraft parameters.

Item	Symbol	Value
Mass	$m$	1200 kg
Projected area	$A$	3000 m <sup>2</sup>
Moments of Inertia	$I_x, I_y$	$8.24 \times 10^4$ kg · m <sup>2</sup>
	$I_z$	$1.64 \times 10^5$ kg · m <sup>2</sup>
Optical constants	$C_s, C_d, C_a$	0.2, 0.1, 0.7

Table 2. Small body parameters.

Item	Symbol	Value
Distance from the Sun	$d$	5.2 AU
Mean diameter		20 km
Axis ratio	$R_a : R_b : R_c$	1.4 : 1.2 : 1
Density		2.0 g/cm <sup>3</sup>
Rotation period	$T_{rot}$	10 hr

of the Sun, that is, the normal direction of the surface where solar cells are mounted.  $C_s$ ,  $C_d$ , and  $C_a$  are optical constants of the spacecraft surface that correspond to the modes of specular reflection, diffuse reflection, and absorption, respectively, which satisfy  $C_s + C_d + C_a = 1$ .

The physical parameters for a small body are given in Table 2. This study assumes a hypothetical Trojan asteroid that is moving in a circular orbit, with a radius of 5.2 AU, around the Sun. The body is modeled as a homogeneous triaxial ellipsoid, with a mean diameter of 20 km, rotating uniformly about the shortest axis. This rotation axis is assumed to be perpendicular to the ecliptic plane. The rotation axis can take any direction in general; however, it has been observed that near Earth asteroids and main belt asteroids with small diameters ( $\leq 30$  km) are more likely to have a small obliquity.<sup>5,19,20)</sup> Although detailed discussions are required to directly apply the theory to Trojan asteroids, this assumption regarding the rotation axis is made for initial analyses in this study.

### 2.2. Coordinate system

To describe the orbital and attitude motions of a spacecraft, six different coordinate systems are used, as shown in Fig. 3.

**Inertial coordinate:**  $(x^I, y^I, z^I)$  A right-handed Cartesian coordinate system that is fixed in the inertial space.

**Hill coordinate:**  $(x^H, y^H, z^H)$  The origin is at the center of a small body. The  $x$  axis points in the anti-Sun direction, the  $z$  axis is aligned with the angular velocity vector of the orbit of the small body around the Sun, and the  $y$  axis completes a right-handed Cartesian coordinate system.

**Small-body-fixed coordinate:**  $(x^{SB}, y^{SB}, z^{SB})$  The  $x$ ,  $y$ , and  $z$  axes are fixed on the longest, intermediate, and shortest axis, respectively, of the small body. The  $z$  axis is identical to  $z^H$  because of the assumption given in the previous subsection.

**Sun-pointing coordinate:**  $(x^{SP}, y^{SP}, z^{SP})$  The origin is at the center of the spacecraft. The  $z$  axis points in the Sun direction, the  $x$  axis is parallel to the plane formed by  $x^H$  and  $y^H$ , and the  $y$  axis completes a right-handed Cartesian coordinate system.

**Spacecraft-fixed coordinate:**  $(x^{SC}, y^{SC}, z^{SC})$  The origin is at the center of the spacecraft. All axes are fixed on the spacecraft and are aligned along the principal directions.

Spin-free coordinate:  $(x^{SF}, y^{SF}, z^{SF})$  The origin is at the center of the spacecraft. The  $z$  axis is identical to  $z^{SC}$ , the  $x$  axis is parallel to the plane formed by  $x^{SP}$  and  $y^{SP}$ , and the  $y$  axis completes a right-handed Cartesian coordinate system.

From these definitions, the attitude of the spacecraft can be expressed by Euler angles  $(\theta, \phi, \psi)$ , considering a 2-1-3 rotation sequence from the Sun-pointing coordinate to the spacecraft-fixed coordinate. Because the distance between the small body and the spacecraft is sufficiently smaller than that between the Sun and the small body,  $\theta$  and  $\phi$  can be regarded as in-plane and out-of-plane Sun angles with respect to the ecliptic plane.

Let  ${}^A\mathbf{u}$  denote a 3-dimensional vector in an arbitrary  $A$ -coordinate system, and let  ${}^B\mathbf{C}_A$  denote the rotational transformation matrix from an  $A$ -coordinate to an  $B$ -coordinate system. Then, the rotational coordinate transformation for the vector is expressed as  ${}^B\mathbf{u} = {}^B\mathbf{C}_A {}^A\mathbf{u}$ . The rotational coordinate transformation matrices between some of the coordinate systems are given in the following paragraphs. Here, the rotational transformation matrices about the  $x$ ,  $y$ , and  $z$  axes by an angle  $\theta$  are denoted as  $\mathbf{R}_x(\theta)$ ,  $\mathbf{R}_y(\theta)$ , and  $\mathbf{R}_z(\theta)$ .

When the rotation angle of a small body with respect to the Hill coordinate is denoted by  $\theta_{rot}$ , as shown in Fig. 3, the rotational transformation from the Hill coordinate to the small-body-fixed coordinate is given by the equation below.

$${}^S\mathbf{C}_H = \mathbf{R}_z(\theta_{rot}) \quad (1)$$

Let  $(x, y, z)$  denote the position of the spacecraft in terms of the Hill coordinate, and  $d$  denote the distance between the Sun and a small body. Because  $x, y, z \ll d$  holds in the proximity of the small body, the rotational transformation from the Hill coordinate to the Sun-pointing coordinate is given by the following equation:

$${}^{SP}\mathbf{C}_H \approx \mathbf{R}_x\left(-\frac{\pi}{2}\right)\mathbf{R}_z\left(\frac{\pi}{2}\right) \quad (2)$$

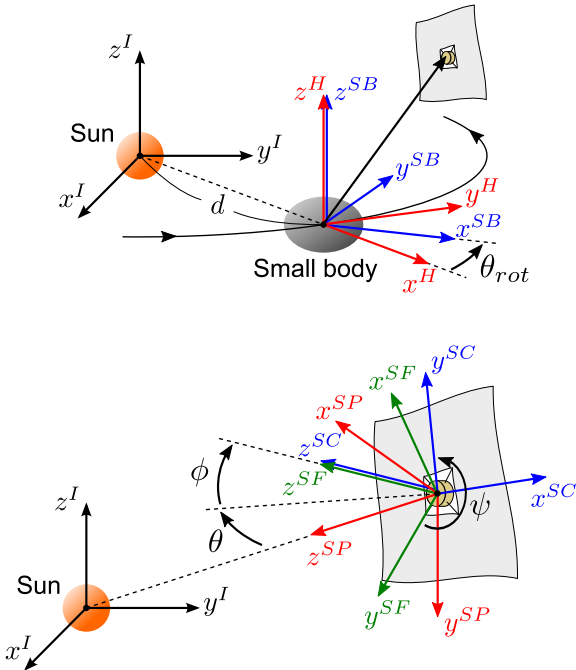


Fig. 3. Coordinate systems.

Considering a 2-1-3 rotation sequence with a rotation angle set of  $(\theta, \phi, 0)$ , the rotational transformation from the Sun-pointing coordinate to the spin-free coordinate is expressed as follows:

$${}^{SF}\mathbf{C}_{SP} = \mathbf{R}_x(\phi)\mathbf{R}_y(\theta) \quad (3)$$

On the other hand, a 2-1-3 rotation sequence with a rotation angle set of  $(\theta, \phi, \psi)$  corresponds to the rotational transformation from the Sun-pointing coordinate to the spacecraft-fixed coordinate, which is given by the following equations:

$${}^{SC}\mathbf{C}_{SF} = \mathbf{R}_z(\psi) \quad (4)$$

$${}^{SC}\mathbf{C}_{SP} = {}^{SC}\mathbf{C}_{SF} {}^{SF}\mathbf{C}_{SP} = \mathbf{R}_z(\psi)\mathbf{R}_x(\phi)\mathbf{R}_y(\theta) \quad (5)$$

### 2.3. Gravity model

The gravity of a small body is calculated based on an triaxial ellipsoid model. Let  $U_{G,C_{00}}$ ,  $U_{G,C_{2k}}$ , and  $U_{G,C_{4k}}$  denote the gravitational potential of a mass element due to the zeroth-, second-, and fourth-order gravity terms;  $\mathbf{R}$  denote the relative position vector of a mass element with respect to the center of mass of the small body;  $\mathbf{r}$  denote the relative position vector of the center of mass of the spacecraft relative to that of the small body; and  $\boldsymbol{\rho}$  denote the relative position vector of the element relative to the center of mass of the spacecraft. The geometric relations between the position vectors are illustrated in Fig. 4.

Considering the derivative of the gravitational potentials with respect to  $\mathbf{R}$ , the gravitational force and the GG torque can be expressed by Eqs. (6) and (7).

$$\mathbf{F}_G = \int \frac{\partial U_{G,C_{00}}}{\partial \mathbf{R}} dm + \int \frac{\partial U_{G,C_{2k}}}{\partial \mathbf{R}} dm + m \left. \frac{\partial U_{G,C_{4k}}}{\partial \mathbf{R}} \right|_{\mathbf{R}=\mathbf{r}} \quad (6)$$

$$\mathbf{T}_{GG} = \int \boldsymbol{\rho} \times \frac{\partial U_{G,C_{00}}}{\partial \mathbf{R}} dm + \int \boldsymbol{\rho} \times \frac{\partial U_{G,C_{2k}}}{\partial \mathbf{R}} dm \quad (7)$$

These equations assume that the gravitational potential up to the fourth order contributes to the force acting on the spacecraft, while the potential up to the second order contributes to the torque. In Eq. (6), the spacecraft is treated as a point mass for the calculation of the gravitational force due to the fourth-order terms. By contrast, the shape of the spacecraft is taken into account for the force due to the zeroth- and second-order terms, which means that the attitude of the spacecraft exerts influence on the orbital motion, thereby causing the gravitational coupling effect. The explicit formulations of  $U_{G,C_{00}}$ ,  $U_{G,C_{2k}}$ ,  $U_{G,C_{4k}}$ ,  $\mathbf{F}_G$ , and  $\mathbf{T}_{GG}$  are provided in our previous paper.<sup>11)</sup>

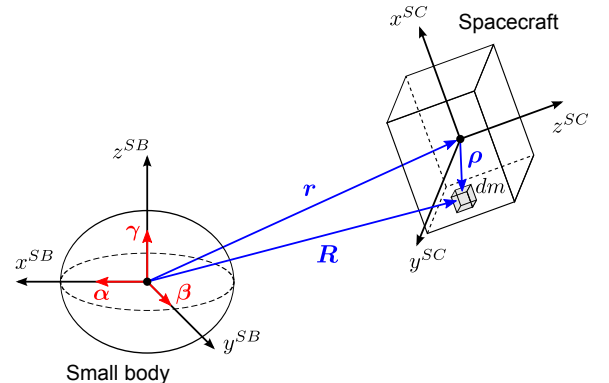


Fig. 4. Position of a spacecraft relative to a small body.

### 3. Solar radiation pressure model

The formulations of SRP force and SRP torque acting on a spacecraft with non-flat surfaces are derived in this section. When the surface of a spacecraft is deformed, the effect of SRP differs from that of an ideal flat surface. One of the most comprehensive models proposed in preceding research is the Generalized Sail Model, which is applicable to solar sail spacecraft with arbitrary shapes and optical parameters.<sup>21,22)</sup> The more simplified model has been constructed for spinning solar sails that is referred to as the Generalized Spinning Sail Model (GSSM).<sup>16)</sup> The GSSM serves as a valid model for spacecraft with axisymmetrical shapes and spin-stabilized spacecraft that are assumed to be axisymmetrical by applying spin-averaging. This model has been exploited to investigate the attitude motion of solar sail spacecraft subject to SRP torque. In addition to the torque model, this paper derives an SRP force model by extending the GSSM theories in order to analyze the orbital motion as well.

#### 3.1. Derivations of force and torque models

The SRP force  $d\mathbf{F}_{SRP}$  acting on a sail element  $dA$  on the membrane is expressed by the equation below.<sup>16,23)</sup>

$$d\mathbf{F}_{SRP} = -P(\mathbf{n} \cdot \mathbf{s})\{(2(\mathbf{n} \cdot \mathbf{s})C_s + B_f C_d)\mathbf{n} + (C_d + C_a)\mathbf{s}\}dA \quad (8)$$

Here,  $\mathbf{n}$  is a unit vector normal to the sail element;  $\mathbf{s}$  is a unit vector pointing from the spacecraft to the Sun;  $B_f = 2/3$  is the Lambertian coefficient; and  $P = P_0/d^2$  is the SRP acting on the surface of the spacecraft, where  $P_0 \approx 1 \times 10^{17} \text{ kg m/s}^2$  is the solar flux constant.<sup>24)</sup> Note that the vector  $\mathbf{n}$  is given such that  $\mathbf{n} \cdot \mathbf{s} \geq 0$  is satisfied. The sail element  $dA$  and the unit vectors  $\mathbf{n}$  and  $\mathbf{s}$  are depicted in Fig. 5. Let  $\kappa_1$ ,  $\kappa_2$ , and  $\kappa_3$  be defined as follows:

$$\kappa_1 = 2C_s, \quad \kappa_2 = B_f C_d, \quad \kappa_3 = C_d + C_a \quad (9)$$

Then, the SRP force exerted on a spacecraft is expressed by the equation below.

$$\begin{aligned} \mathbf{F}_{SRP} &= \int d\mathbf{F}_{SRP} \\ &= \mathbf{F}_{SRP,1} + \mathbf{F}_{SRP,2} + \mathbf{F}_{SRP,3} \end{aligned} \quad (10)$$

where

$$\begin{aligned} \mathbf{F}_{SRP,1} &\equiv -P\kappa_1 \int (\mathbf{n} \cdot \mathbf{s})^2 \mathbf{n} dA \\ \mathbf{F}_{SRP,2} &\equiv -P\kappa_2 \int (\mathbf{n} \cdot \mathbf{s}) \mathbf{n} dA \\ \mathbf{F}_{SRP,3} &\equiv -P\kappa_3 \int (\mathbf{n} \cdot \mathbf{s}) \mathbf{s} dA \end{aligned} \quad (11)$$

In the same manner, the SRP torque can be calculated from the following equation.

$$\begin{aligned} \mathbf{T}_{SRP} &= \int \boldsymbol{\rho} \times d\mathbf{F}_{SRP} \\ &= \mathbf{T}_{SRP,1} + \mathbf{T}_{SRP,2} + \mathbf{T}_{SRP,3} \end{aligned} \quad (12)$$

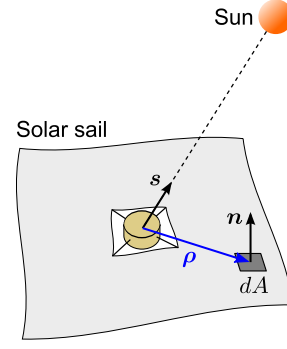


Fig. 5. Sail element on the membrane of a solar sail spacecraft.

where

$$\begin{aligned} \mathbf{T}_{SRP,1} &\equiv -P\kappa_1 \int \boldsymbol{\rho} \times (\mathbf{n} \cdot \mathbf{s})^2 \mathbf{n} dA \\ \mathbf{T}_{SRP,2} &\equiv -P\kappa_2 \int \boldsymbol{\rho} \times (\mathbf{n} \cdot \mathbf{s}) \mathbf{n} dA \\ \mathbf{T}_{SRP,3} &\equiv -P\kappa_3 \int \boldsymbol{\rho} \times (\mathbf{n} \cdot \mathbf{s}) \mathbf{s} dA \end{aligned} \quad (13)$$

The vectors  $\boldsymbol{\rho}$  and  $\mathbf{s}$  can be expressed in the spacecraft-fixed coordinate by the equations below.

$${}^{SC}\boldsymbol{\rho} = \begin{bmatrix} \rho \cos \sigma \\ \rho \sin \sigma \\ \zeta \end{bmatrix}, \quad {}^{SC}\mathbf{s} = \begin{bmatrix} s_x \\ s_y \\ s_z \end{bmatrix} \quad (14)$$

Then, the normal vector  $\mathbf{n}$  is derived as

$${}^{SC}\mathbf{n} = \frac{\partial \boldsymbol{\rho}}{\partial \rho} \times \frac{\partial \boldsymbol{\rho}}{\rho \partial \sigma} = \begin{bmatrix} -\frac{\partial \zeta}{\partial \rho} \cos \sigma + \frac{\partial \zeta}{\rho \partial \sigma} \sin \sigma \\ -\frac{\partial \zeta}{\partial \rho} \sin \sigma - \frac{\partial \zeta}{\rho \partial \sigma} \cos \sigma \\ 1 \end{bmatrix} \quad (15)$$

An arbitrary axisymmetrical or spinning spacecraft can be reduced to an equivalent simplified model on the basis of the following assumptions:<sup>16)</sup>

$$\begin{aligned} \eta &= \frac{\partial \zeta}{\partial \rho} = \text{const.} \ll 1, \quad \xi = \frac{\partial \zeta}{\rho \partial \sigma} = \text{const.} \ll 1, \\ \zeta(\rho) &= h + \rho\eta, \quad h \ll R_{sc}, \\ p_1 &= \text{const.}, \quad p_2 = \text{const.}, \quad p_3 = \text{const.} \end{aligned} \quad (16)$$

Figure 6 depicts the reduced model based on the GSSM and the physical implications of the sail parameters. The deformation of a sail is characterized by two parameters: the outer-plane deformation angle  $\eta$  and the torsion angle  $\xi$ .  $R_{sc}$  is the equivalent sail radius, which satisfies  $A = \pi R_{sc}^2$ , and  $h$  is the offset of the sail attachment from the center of mass of the spacecraft.

A sail element  $dA$  can be expressed by the equation below.

$$dA = \rho d\rho d\sigma \quad (17)$$

Then, the SRP force applied to a spacecraft is derived as follows from Eqs. (10) and (11) by neglecting higher-order terms of  $\eta$  and  $\xi$ .

$$\begin{aligned} {}^{SC}\mathbf{F}_{SRP} &= -\frac{PA}{2} \times \\ &\begin{bmatrix} (2\kappa_1 s_z + \kappa_2)(\eta^2 + \xi^2)s_x + 2\kappa_3 s_x s_z \\ (2\kappa_1 s_z + \kappa_2)(\eta^2 + \xi^2)s_y + 2\kappa_3 s_y s_z \\ 2(\kappa_1 s_z + \kappa_2 + \kappa_3 s_z)s_z + \kappa_3(\eta^2 + \xi^2)(s_x^2 + s_y^2) \end{bmatrix} \end{aligned} \quad (18)$$

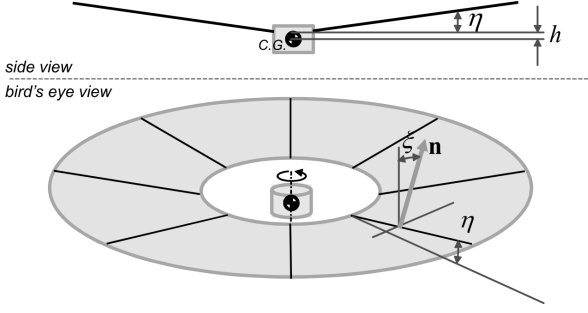


Fig. 6. Reduced model equivalent of an arbitrary spinning spacecraft based on the GSSM.<sup>16)</sup>

Likewise, the SRP torque acting on a spacecraft is calculated as follows from Eqs. (12) and (13).<sup>16)</sup>

$${}^{SC}T_{SRP} = \frac{PAR_{sc}}{3} \times \begin{bmatrix} -(2\kappa_1 s_z + \kappa_2 + \kappa_3 s_z)(\xi s_x - \eta s_y) + \kappa_3 s_y s_z \left(2\eta + \frac{3h}{R_{sc}}\right) \\ -(2\kappa_1 s_z + \kappa_2 + \kappa_3 s_z)(\eta s_x + \xi s_y) - \kappa_3 s_x s_z \left(2\eta + \frac{3h}{R_{sc}}\right) \\ 2(\kappa_1 s_z + \kappa_2)\xi s_z + \kappa_3 \xi (s_x^2 + s_y^2) \end{bmatrix} \quad (19)$$

Once the direction of the Sun is specified in terms of the spacecraft-fixed coordinate, that is  ${}^{SC}s = [s_x, s_y, s_z]^T$ , then the force and torque due to SRP can be computed from Eqs. (18) and (19). These equations indicate that the SRP force and torque are governed by the parameters  $\eta$  and  $\xi$ , and the SRP torque depends on the parameter  $h$  as well. It is to be noted that substitution of  $\eta = \xi = 0$  into Eqs. (18) and (19) yields the SRP force and torque exerted on a spacecraft with an ideal flat surface.

### 3.2. Linearization of the torque model

Assuming that Sun-tracking attitude motion is achieved and the  $z^{SC}$  axis is directed close to the Sun, the equations below hold true.

$$s_x, s_y \ll 1 \quad \text{and} \quad s_z \simeq 1 \quad (20)$$

Based on this assumption, Eq.(19) is linearized as follows:

$${}^{SC}T_{SRP} \simeq \frac{PAR_{sc}}{3} \times \begin{bmatrix} -(2\kappa_1 + \kappa_2 + \kappa_3)(\xi s_x - \eta s_y) + \kappa_3 s_y \left(2\eta + \frac{3h}{R_{sc}}\right) \\ -(2\kappa_1 + \kappa_2 + \kappa_3)(\eta s_x + \xi s_y) - \kappa_3 s_x \left(2\eta + \frac{3h}{R_{sc}}\right) \\ 2(\kappa_1 + \kappa_2)\xi s_z \end{bmatrix} \quad (21)$$

$$= \frac{PAR_{sc}}{3} \begin{bmatrix} -b_2 & b_1 & 0 \\ -b_1 & -b_2 & 0 \\ 0 & 0 & b_3 \end{bmatrix} \begin{bmatrix} s_x \\ s_y \\ s_z \end{bmatrix} \quad (22)$$

where

$$\begin{aligned} b_1 &= (2\kappa_1 + \kappa_2 + 3\kappa_3)\eta + 3\kappa_3 \frac{h}{R_{sc}} \\ b_2 &= (2\kappa_1 + \kappa_2 + \kappa_3)\xi \\ b_3 &= 2(\kappa_1 + \kappa_2)\xi \end{aligned} \quad (23)$$

Let a matrix  $\mathbf{B}$  be defined as follows:

$${}^{SC}\mathbf{B} = \frac{PAR_{sc}}{3} \begin{bmatrix} -b_2 & b_1 & 0 \\ -b_1 & -b_2 & 0 \\ 0 & 0 & b_3 \end{bmatrix} \quad (24)$$

Considering the form of Eq. (22), the SRP torque acting on a spacecraft is expressed in a general form by the linearized equation below.

$$\mathbf{T}_{SRP} \simeq \mathbf{B}\mathbf{s} \quad (25)$$

To comprehend the dynamics regarding the Sun angles  $\theta$  and  $\phi$ , the following part derives the SRP torque in terms of the spin-free coordinate system.  $\mathbf{B}$  and  $\mathbf{s}$  are expressed in the spin-free coordinate as follows:

$${}^{SF}\mathbf{B} = ({}^{SC}\mathbf{C}_{SF})^T {}^{SC}\mathbf{B} {}^{SC}\mathbf{C}_{SF} = {}^{SC}\mathbf{B} \quad (26)$$

$${}^{SF}\mathbf{s} = {}^{SF}\mathbf{C}_{SP} {}^{SP}\mathbf{s} \simeq \begin{bmatrix} -\theta \\ \phi \\ 1 \end{bmatrix} \quad (27)$$

From Eqs. (25)–(27), the SRP torque based on the GSSM is formulated by the following equation:

$${}^{SF}\mathbf{T}_{SRP} \simeq \frac{PAR_{sc}}{3} \begin{bmatrix} b_1\phi + b_2\theta \\ -b_2\phi + b_1\theta \\ b_3 \end{bmatrix} \quad (28)$$

It is important to reiterate that  $\phi$  and  $\theta$  are assumed to be sufficiently small, such that Eq. (28) is linearized with respect to  $\phi$  and  $\theta$ .

## 4. Orbital motion

This section provides Sun-synchronous orbit solutions that are solved by an analytical approach based on Lagrange planetary equations. Although the solutions have been derived in previous research and this part is not the contribution of the present study, the derivation of the solutions is presented for the sake of clarity in subsequent sections.

### 4.1. Lagrange planetary equations

The most predominant gravity-irregularity effect stems from the  $C_{20}$  term, in general, which corresponds to the oblateness of a gravitational mass. The orbital motion of a spacecraft subject to SRP perturbation and the oblateness effect is expressed by the following averaged Lagrange planetary equations:<sup>5,11)</sup>

$$\begin{aligned} \frac{da}{dt} &= 0 \\ \frac{de}{dt} &= -K_{SRP} \sqrt{1-e^2} (\sin \omega \cos \Omega + \cos \omega \sin \Omega \cos i) \\ \frac{di}{dt} &= -K_{SRP} \frac{e}{\sqrt{1-e^2}} \cos \omega \sin \Omega \sin i \\ \frac{d\Omega}{dt} &= -K_{SRP} \frac{e}{\sqrt{1-e^2}} \sin \omega \sin \Omega + \frac{K_{J_2}}{(1-e^2)^2} \cos i - N \\ \frac{d\omega}{dt} &= -\frac{K_{SRP}}{e\sqrt{1-e^2}} \{(1-e^2) \cos \omega \cos \Omega - \sin \omega \sin \Omega \cos i\} \\ &\quad + \frac{K_{J_2}}{(1-e^2)^2} \left( \frac{5}{2} \sin^2 i - 2 \right) \end{aligned} \quad (29)$$

Table 3. Parameters of the ideal Sun-synchronous orbit.

Item	Symbol	Value
Semi-major axis	$a$	60 km
Eccentricity	$e$	0.0547
Inclination	$i$	90.91 deg
Longitude of the ascending node	$\Omega$	-90 deg
Argument of periapsis	$\omega$	90 deg
Period	$\tau$	1.429 days

where  $(a, e, i, \Omega, \omega)$  denotes the set of orbital elements defined in the Hill coordinate;  $N$  denotes the mean motion of a small body; and  $K_{J_2}$  and  $K_{SRP}$  are functions of the semi-major axis  $a$ , as follows:

$$K_{J_2} = \frac{3}{2} \frac{\sqrt{\mu} C_{20} R_a^2}{a^{\frac{7}{2}}}, \quad K_{SRP} = \frac{3}{2} \frac{|\mathbf{F}_{SRP,0}|}{m} \sqrt{\frac{a}{\mu}} \quad (30)$$

Here,  $\mathbf{F}_{SRP,0}$  represents the SRP force for the case where the Sun angles are zero. This formulation assumes that the  $z^{SC}$  axis of the spacecraft is constantly directed toward the Sun.  $\mathbf{F}_{SRP,0}$  is obtained from Eq. (18) by substituting  $s_x = s_y = 0$  and  $s_z = 1$ .

#### 4.2. Sun-synchronous orbit solutions

Sun-synchronous frozen orbits can be achieved when all of the derivatives of orbital elements described in Eq. (29) are equal to zero. Several types of orbits are known to satisfy this condition. The present study investigates one of these orbits, called a near-polar terminator orbit, because this type of orbit can avoid solar eclipse and has relatively small eccentricity.<sup>5)</sup> The orbital elements of near-polar terminator orbits can be solved as follows:

$$\begin{aligned} a &= \text{free}, \quad e = f_1(a), \quad i = f_2(a) \\ \Omega &= \pm \frac{\pi}{2}, \quad \omega = \mp \frac{\pi}{2} \end{aligned} \quad (31)$$

Here,  $f_1(a)$  and  $f_2(a)$  are implicit functions of the semi-major axis obtained by solving the following equations numerically:

$$\begin{aligned} K_{SRP} \frac{e}{\sqrt{1-e^2}} + \frac{K_{J_2}}{(1-e^2)^2} \cos i - N &= 0 \\ \frac{K_{SRP}}{e\sqrt{1-e^2}} \cos i - \frac{K_{J_2}}{(1-e^2)^2} \left( \frac{5}{2} \sin^2 i - 2 \right) &= 0 \end{aligned} \quad (32)$$

An example of a Sun-synchronous orbit around the small body expressed in the Hill coordinate system is presented in Fig. 7, and the corresponding orbital elements are provided in Table 3. The semi-major axis is given as 60 km, and the eccentricity and inclination are solved from Eq. (32). This orbit is solved for a spacecraft with an ideal flat surface that satisfies  $\eta = \xi = 0$ . The result demonstrates that the solution of a Sun-synchronous orbit actually exists, even when both the SRP perturbation and the gravity irregularity are predominant. Note that Fig. 7 merely shows an ideal elliptic orbit that is not the result of numerical integration.

## 5. Attitude motion

### 5.1. Linearized Euler equation

Attitude motion of a spacecraft observed in the spacecraft-fixed or spin-free coordinate is expressed by the Euler equations below.

$$\mathbf{I} \frac{d\boldsymbol{\omega}_{SC/I}}{dt} \Big|_A = -\boldsymbol{\omega}_{A/I} \times \mathbf{I} \boldsymbol{\omega}_{SC/I} + \mathbf{T} \quad (33)$$

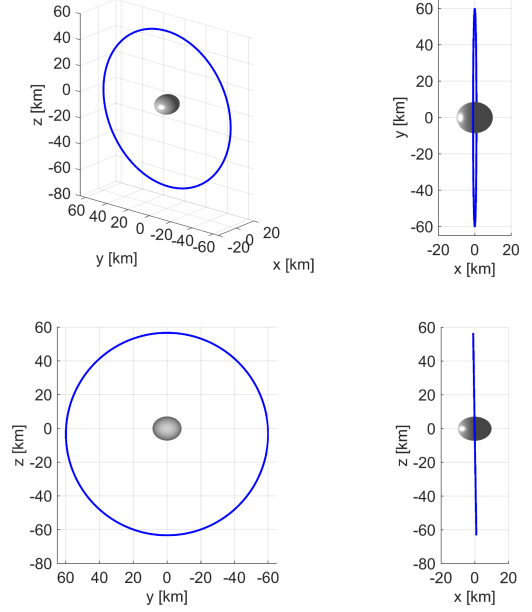


Fig. 7. Example of a Sun-synchronous orbit.

where  $d/dt|_A$  represents the time derivative in an  $A$ -coordinate system;  $\boldsymbol{\omega}_{A/B}$  denotes the angular velocity vector of an  $A$ -coordinate system relative to a  $B$ -coordinate system;  $\mathbf{T}$  is the sum of external torques acting on a spacecraft; and  $\mathbf{I}$  is the moment of inertia tensor which can be expressed as follows because of the axisymmetry:

$${}^{SC}\mathbf{I} = \begin{bmatrix} I_x & 0 & 0 \\ 0 & I_y & 0 \\ 0 & 0 & I_z \end{bmatrix}, \quad {}^{SF}\mathbf{I} = \begin{bmatrix} I_r & 0 & 0 \\ 0 & I_r & 0 \\ 0 & 0 & I_z \end{bmatrix} \quad (34)$$

where  $I_r \equiv I_x = I_y$ . Assuming that  $\phi, \theta \ll 1$  holds, the equation of attitude motion expressed in the spin-free coordinate is linearized as the following equation:<sup>11)</sup>

$$\begin{bmatrix} I_r \ddot{\phi} \\ I_r \ddot{\theta} \\ I_z \ddot{\Omega}_z \end{bmatrix} = \begin{bmatrix} -I_z \Omega_z (\dot{\theta} - N) \\ I_z \Omega_z \dot{\phi} \\ 0 \end{bmatrix} + {}^{SF}\mathbf{T}_{GG} + {}^{SF}\mathbf{T}_{SRP} \quad (35)$$

where  ${}^{SF}\boldsymbol{\omega}_{SC/SF} = [0, 0, \Omega_z]^T$ .

If the GG torque due to higher-order gravity terms is neglected for simplicity,  $\mathbf{T}_{GG}$  can be expressed as follows, based on Eq. (7):

$$\mathbf{T}_{GG} = \frac{3\mu}{|\mathbf{r}|^5} \mathbf{r} \times \mathbf{I} \mathbf{r} \quad (36)$$

When a Sun-synchronous frozen orbit is achieved, position vector  $\mathbf{r}$  is expressed explicitly as a function of the true anomaly. In such a case, the GG torque can be averaged over one period of the orbit around a small body as given by the equation below.<sup>11)</sup>

$${}^{SF}\overline{\mathbf{T}}_{GG} = \frac{3\mu(I_z - I_r)}{4a^3(1-e^2)^{\frac{3}{2}}} \begin{bmatrix} c_1\phi + c_2\theta + c_4 \\ c_2\phi + c_3\theta + c_5 \\ 0 \end{bmatrix} \quad (37)$$

where

$$\begin{aligned} c_1 &= 2(-\sin^2 i \sin^2 \Omega + \cos^2 i), \quad c_2 = -\sin 2i \cos \Omega \\ c_3 &= 2 \sin^2 i \cos 2\Omega, \quad c_4 = -\sin 2i \sin \Omega, \quad c_5 = \sin^2 i \sin 2\Omega \end{aligned} \quad (38)$$

Substitution of Eqs. (28) and (37) into Eq. (35) yields a linear differential equation in terms of  $\phi$  and  $\theta$ .

## 5.2. Stability conditions of Sun-tracking attitude motion

The attitude motion of a spacecraft is composed of a low frequency component called precession and a high frequency component called nutation. In general, the time dependence of precession is much slower than nutation. Therefore, when the nutation motion is ignored such that only the precession motion is considered, the change rates of  $\phi$  and  $\theta$  can be approximated as constant, yielding  $\dot{\phi} \approx \dot{\theta} \approx 0$ .<sup>16)</sup> This assumption is also valid for the case where the spacecraft is in pure rotation.<sup>10)</sup> Then, considering the first and second components of Eq. (35), the equation is simplified to a first-order differential equation as follows:

$$I_z \Omega_z \begin{bmatrix} \dot{\theta} \\ \dot{\phi} \end{bmatrix} = \begin{bmatrix} I_z \Omega_z N \\ 0 \end{bmatrix} + \begin{bmatrix} {}^{SF} \bar{T}_{GG,x} \\ -{}^{SF} \bar{T}_{GG,y} \end{bmatrix} + \begin{bmatrix} {}^{SF} T_{SRP,x} \\ -{}^{SF} T_{SRP,y} \end{bmatrix} \quad (39)$$

From Eqs. (28) and (37), Eq. (39) can be rewritten as the equation below.

$$\begin{bmatrix} \dot{\theta} \\ \dot{\phi} \end{bmatrix} = \frac{1}{I_z \Omega_z} \left( \begin{bmatrix} C_2 & C_1 \\ -C_4 & -C_3 \end{bmatrix} \begin{bmatrix} \theta \\ \phi \end{bmatrix} + \begin{bmatrix} C_5 + I_z \Omega_z N \\ -C_6 \end{bmatrix} \right) \quad (40)$$

where

$$p = \frac{PAR_{sc}}{3}, \quad q = \frac{3\mu(I_z - I_r)}{4a^3(1 - e^2)^{\frac{3}{2}}} \quad (41)$$

$$C_1 = pb_1 + qc_1, \quad C_2 = pb_2 + qc_2, \quad C_3 = -pb_2 + qc_2$$

$$C_4 = pb_1 + qc_3, \quad C_5 = qc_4, \quad C_6 = qc_5$$

The equilibrium attitude state is solved by substituting  $\dot{\phi} = \dot{\theta} = 0$  into Eq. (40), as follows:

$$\phi_{eq} = \frac{C_2 C_6 - C_4 (C_5 + I_z \Omega_z N)}{C_1 C_4 - C_2 C_3} \quad (42)$$

$$\theta_{eq} = \frac{-C_1 C_6 + C_3 (C_5 + I_z \Omega_z N)}{C_1 C_4 - C_2 C_3}$$

The stability of the motion around an equilibrium point is investigated on the basis of the characteristic equation below.

$$\lambda^2 + \alpha\lambda + \beta = 0 \quad (43)$$

Here,  $\lambda$  represents the eigenvalues of the  $2 \times 2$  matrix in Eq. (40), and  $\alpha$  and  $\beta$  are defined as follows:

$$\alpha = -\frac{1}{I_z \Omega_z} (C_2 - C_3) \quad (44)$$

$$\beta = \frac{1}{(I_z \Omega_z)^2} (C_1 C_4 - C_2 C_3)$$

The attitude motion exhibits stability when both of the eigenvalues possess non-positive real component. Thus, the necessary and sufficient condition to achieve stability is expressed by the two inequalities below.<sup>25)</sup>

$$\alpha > 0 \quad \text{and} \quad \beta > 0 \quad (45)$$

Both stable and unstable motions can be categorized into spirals and nodes, depending on the sign of  $\Delta = \alpha^2 - 4\beta$ . Figure 8 shows a phase plane that visualizes the classification of the modes of attitude stability, which include center, spiral, node, and saddle. The gray region in the figure corresponds to the stable cases.

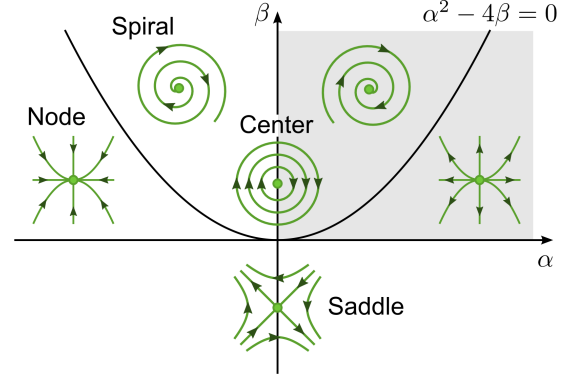


Fig. 8. Phase plane and classification for the attitude stability.<sup>25)</sup>

## 6. Coupled orbit-attitude motion

### 6.1. Hill's equation and Euler equation

Orbital motion is modeled by the Lagrange planetary equation in Section 4, and attitude motion is analyzed by the linearized Euler equation in Section 5. Although these models enable analytical analyses to comprehend the fundamental dynamics behind the complex orbit-attitude coupled system, they are formulated with approximations that involve linearization and averaging. Therefore, this section investigates non-linear orbit-attitude coupled dynamics to demonstrate the validity of the analytical theories established in the previous sections.

The orbital motion of a spacecraft in the vicinity of a small body moving in a circular orbit around the Sun can be modeled as Hill's equation below.<sup>24,26)</sup>

$$m \begin{bmatrix} \ddot{x} \\ \ddot{y} \\ \ddot{z} \end{bmatrix} = m \begin{bmatrix} 2N\dot{y} + 3N^2x \\ -2N\dot{x} \\ -N^2z \end{bmatrix} + {}^H F_G + {}^H F_{SRP} \quad (46)$$

Here,  $N = |\omega_{H/I}|$  is the mean motion of a small body. The gravitational force  ${}^H F_G$  and the SRP force  ${}^H F_{SRP}$  are calculated from Eqs. (6) and (18), which incorporate the effect of the attitude motion of a spacecraft.

On the other hand, the attitude motion is described by Eq. (33), and the motion observed in the spacecraft-fixed coordinate is given by the equation below.

$$\begin{bmatrix} I_x \dot{\omega}_x \\ I_y \dot{\omega}_y \\ I_z \dot{\omega}_z \end{bmatrix} = \begin{bmatrix} (I_y - I_z) \omega_y \omega_z \\ (I_z - I_x) \omega_x \omega_z \\ (I_x - I_y) \omega_x \omega_y \end{bmatrix} + {}^{SC} T_{GG} + {}^{SC} T_{SRP} \quad (47)$$

where  ${}^{SC} \omega_{SC/I} = [\omega_x, \omega_y, \omega_z]^T$ . The GG torque  ${}^{SC} T_{GG}$  and the SRP torque  ${}^{SC} T_{SRP}$  are calculated from Eqs. (7) and (19). Because the GG torque is depending on the position of the spacecraft relative to the small body, Eqs. (46) and (47) form coupled orbit-attitude equations of motion.

Considering a 2-1-3 rotation sequence from the Sun-pointing coordinate to the spacecraft-fixed coordinate with an Euler angle set of  $(\theta, \phi, \psi)$ , a kinematic equation that describes the relationship between angular velocities and Euler angles can be expressed as follows:

$$\begin{bmatrix} \dot{\phi} \\ \dot{\theta} \\ \dot{\psi} \end{bmatrix} = \begin{bmatrix} \omega_x \cos \psi - \omega_y \sin \psi \\ (\omega_x \sin \psi + \omega_y \cos \psi) \sec \phi + N \\ (\omega_x \sin \psi + \omega_y \cos \psi) \tan \phi + \omega_z \end{bmatrix} \quad (48)$$

Here the derivation of this equation is provided in authors' previous work.<sup>11)</sup>

## 6.2. Simulation results

The simulated results obtained for orbit-attitude coupled motion are provided in Figs. 9–11. These results show the coupled motions of a spacecraft orbiting in the Sun-synchronous orbit shown in Fig. 7. The simulations are performed assuming JAXA’s solar power sail for the Trojan asteroid mission. The spin rate of a spacecraft is given by  $\Omega_z = 20$  rpd and the motions are propagated for 350 days. The simulations compare the motions with different sail deformation parameters.

Figure 9 shows the case where a spacecraft has an ideal flat surface (i.e.  $\eta = \xi = 0$ ). Figure 9(a) illustrates the orbital motion in the Hill coordinate and Fig. 9(b) depicts a visual representation of the attitude trajectory in the  $\phi$ - $\theta$  plane, where the origin corresponds to the direction of the Sun. It can be observed from Fig. 9(a) that the orbital shape and geometry remain constant, and thus, this orbit is a Sun-synchronous orbit. On the other hand, Fig. 9(b) indicates that the spacecraft is constantly directed toward the Sun, with a slight oscillation around the equilibrium point which is represented as the magenta point. Here, the blue arrows in Fig. 9(b) represent the torque field calculated from Eq. (40). The attitude motion exhibits marginal stability and the equilibrium point is classified as a center. This result demonstrates that a Sun-synchronous orbit with Sun-tracking attitude motion can actually be achieved. Such a marginally stable Sun-tracking attitude motion has been observed in previous research as well.<sup>11)</sup>

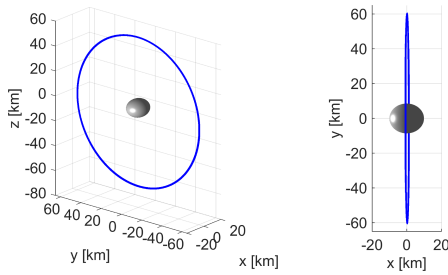
On the other hand, when the surface of a spacecraft is deformed, the orbit-attitude coupled motion shows a unique behavior that has not been observed in past research. Figure 10 illustrates the simulation result for a non-flat solar sail space-

craft that is characterized by a deformation angle  $\eta = -0.5$  deg and a torsion angle  $\xi = -0.2$  deg. These parameters yield  $\alpha = 2.5 \times 10^{-7}$  /s,  $\beta = 3.2 \times 10^{-12}$  /s<sup>2</sup>, and  $\Delta = -1.3 \times 10^{-11}$  /s<sup>2</sup>; therefore, the mode of the attitude motion is a stable spiral, according to the phase plane presented in Fig. 8. The attitude trajectory illustrated in Fig. 10(b) indeed shows a stable spiral motion, which converges to the equilibrium point. This result verifies that analytical theories agree with numerical simulations. Here, this simulation assumes that the torque around the  $z^{SC}$  axis caused by SRP, which is referred to as a windmill torque, is cancelled out by reflectivity control devices such that the spin rate of the spacecraft remains constant.<sup>27)</sup>

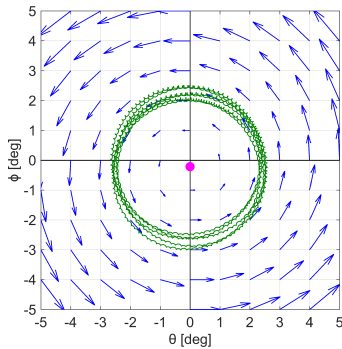
Another simulation result is provided in Fig. 11. The simulation is performed with the same spacecraft and asteroid parameters as those of the case provided in Fig. 10. However, the initial longitude of the ascending node possesses an error of 15 deg in this case. Figures 11(a) and 11(b) illustrate that both orbital motion and attitude motion are significantly disturbed. This observation implies that, in order to achieve a stable orbit-attitude coupled attitude motion under the strongly perturbed environment around a small body, it is essential to fulfill certain initial conditions.

## 7. Conclusion

The present study investigated the implementation of stationary orbit-attitude coupled motion of solar sail spacecraft around small bodies. First, the SRP force and torque acting on a spacecraft with non-flat surfaces has been formulated. On the basis of this SRP model, the analytical conditions to achieve both

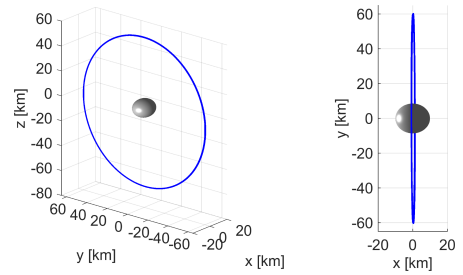


(a) Orbital motion

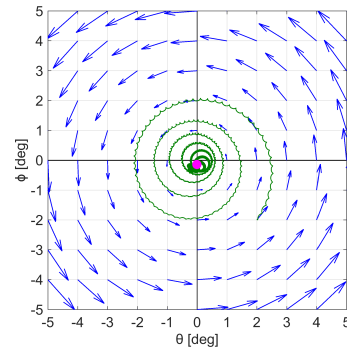


(b) Attitude motion

Fig. 9. Orbit-attitude coupled motion,  $\eta = 0$  and  $\xi = 0$ .

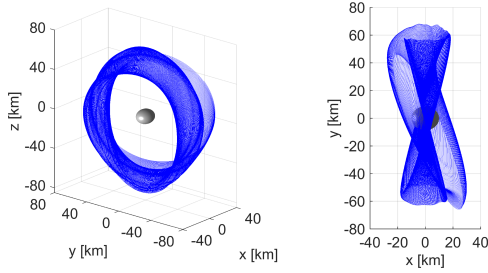


(a) Orbital motion

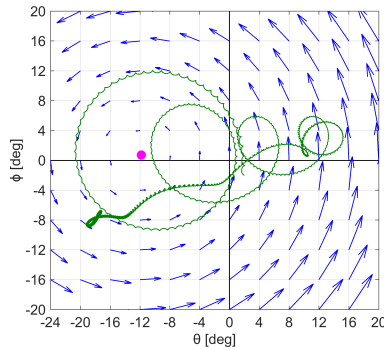


(b) Attitude motion

Fig. 10. Orbit-attitude coupled motion,  $\eta = -0.5$  deg and  $\xi = -0.2$  deg.



(a) Orbital motion



(b) Attitude motion

Fig. 11. Orbit-attitude coupled motion with initial errors.

Sun-synchronous orbits and Sun-tracking attitude motion were successfully derived. The main contribution of this study is to systematically analyze the stability of Sun-tracking attitude motion by introducing a phase plane. According to the phase plane analysis, it was demonstrated that the attitude motion can be classified into several different modes depending on the effects of GG torque and SRP torque.

In addition to analytical analyses, numerical simulations were also performed based on non-linear coupled orbit-attitude equations of motion to verify the validity of the analytical theories. The numerical analyses demonstrated that a spacecraft can maintain its orbital geometry and attitude state with respect to the Sun under a proper condition. Moreover, when the surface of a sail is deformed, the attitude motion exhibits a spiral behavior that has not been observed in our previous study on the orbit-attitude coupled motion around small bodies. From the analyses presented in this paper, it is concluded that the proposed natural orbit-attitude coupled dynamics of solar sail spacecraft is useful for small body missions.

## Acknowledgments

This work was supported by Grant-in-Aid for Scientific Research (15J06932 and 23560964) from the Japan Society for the Promotion of Science.

## References

- 1) Scheeres, D. J.: Satellite Dynamics about Asteroids, *Advances in the Astronautical Sciences*, **87** (1994), pp. 275–292, paper AAS 94-112.
- 2) Scheeres, D. J., Ostro, S. J., Hudson, R. S., Dejong, E. M. and Suzuki,

- S.: Dynamics of Orbits Close to Asteroid 4179 Toutatis, *Icarus*, **132**(1) (1998), pp. 53–79.
- 3) Scheeres, D. J.: Satellite Dynamics about Small Bodies: Averaged Solar Radiation Pressure Effects, *Journal of the Astronautical Sciences*, **47**(1) (1999), pp. 25–46.
- 4) Curtis, H. D.: *Orbital Mechanics for Engineering Students, First edition*, Elsevier Academic Press, Burlington, MA, 2005.
- 5) Lantukh, D., Russell, R. P. and Broschart, S.: Heliotropic Orbits at Oblate Asteroids: Balancing Solar Pressure and J2 Perturbations, *Celestial Mechanics and Dynamical Astronomy*, **121**(2) (2015), pp. 171–190.
- 6) Riverin, J. and Misra, A. K.: Attitude Dynamics of Satellites Orbiting Small Bodies, *AIAA/AAS Astrodynamics Specialist Conference and Exhibit*, , paper AIAA 2002-4520.
- 7) Wang, Y. and Xu, S.: Gravity Gradient Torque of Spacecraft Orbiting Asteroids, *Aircraft Engineering and Aerospace Technology*, **85**(1) (2013), pp. 72–81.
- 8) Wang, Y. and Xu, S.: Attitude Stability of a Spacecraft on a Stationary Orbit around an Asteroid Subjected to Gravity Gradient Torque, *Celestial Mechanics and Dynamical Astronomy*, **115**(4) (2013), pp. 333–352.
- 9) Wang, Y. and Xu, S.: Equilibrium Attitude and Stability of a Spacecraft on a Stationary Orbit around an Asteroid, *Acta Astronautica*, **84** (2013), pp. 99–108.
- 10) Wertz, J. R.: *Spacecraft Attitude Determination and Control, First edition*, Kluwer Academic, Boston, MA, 1978.
- 11) Kikuchi, S., Howell, K. C., Tsuda, Y. and Kawaguchi, J.: Orbit-attitude Coupled Motion around Small Bodies: Sun-synchronous Orbits with Sun-tracking Attitude Motion, *67th International Astronautical Congress*, paper IAC-16-C1.9.2.
- 12) Sincarsin, G. B. and Hughes, P. C.: Gravitational Orbit-Attitude Coupling for Very Large Spacecraft, *Celestial Mechanics*, **31**(2) (1983), pp. 143–161.
- 13) Wang, Y. and Xu, S.: Gravitational Orbit-Rotation Coupling of a Rigid Satellite around a Spheroid Planet, *Journal of Aerospace Engineering*, **27**(1) (2014), pp. 140–150.
- 14) Wang, Y., Xu, S. and Zhu, M.: Stability of Relative Equilibria of the Full Spacecraft Dynamics around an Asteroid with Orbit-Attitude Coupling, *Advances in Space Research*, **53**(7) (2014), pp. 1092–1107.
- 15) Misra, G., Izadi, M., Sanyal, A. and Scheeres, D. J.: Coupled Orbit-Attitude Dynamics and Relative State Estimation of Spacecraft Near Small Solar System Bodies, *Advances in Space Research*, **57**(8) (2016), pp. 1747–1761.
- 16) Tsuda, Y., Saiki, T., Funase, R. and Mimasu, Y.: Generalized Attitude Model for Spinning Solar Sail Spacecraft, *Journal of Guidance, Control, and Dynamics*, **36**(4) (2013), pp. 967–974.
- 17) Mori, O., Saiki, T., Kato, H., Tsuda, Y., Mimasu, Y., Shirasawa, Y., Boden, R., Matsumoto, J., Chujo, T., Kikuchi, S., Kikuchi, J., Oki, Y., Akatsuka, K., Iwata, T., Okada, T., Yano, H., Matsuura, S., Nakamura, R., Kebukawa, Y., Aoki, J. and Kawaguchi, J.: Jovian Trojan Asteroid Exploration by Solar Power Sail-craft, *Trans. JSASS Aerospace Tech. Japan*, **14**(ists30) (2016), pp. Pk1–Pk7.
- 18) Mori, O., Kato, H., Matsumoto, J., Saiki, T., Tsuda, Y., Ogawa, N., Mimasu, Y., Kawaguchi, J., Tanaka, K., Toyota, H., Okuizumi, N., Terui, F., Tomiki, A., Kawasaki, S., Kuninaka, H., and Ryudo Tsukizaki, K. N., Hosoda, S., Bando, N., Yamada, K., Okada, T., Iwata, T., Yano, H., Kebukawa, Y., Aoki, J., Otsuki, M., Nakamura, R., Okamoto, C., Matsuura, S., Yonetoku, D., Matsuoka, A., Nomura, R., Boden, R., Chujo, T., Oki, Y., Takao, Y., Ikemoto, K., Koyama, K., Kinoshita, H., Kitao, S., Nakamura, T., Ishida, H., Umeda, K., Kashioka, S., Kadokura, M., Kurakawa, M. and Watanabe, M.: Direct Exploration of Jupiter Trojan Asteroid using Solar Power Sail, *4th International Symposium on Solar Sailing*, paper 17087.
- 19) Kryszczyńska, A., Spina, A. L., Paolicchi, P., Harris, A. W., Breiter, S. and Pravec, P.: New Findings on Asteroid Spin-Vector Distributions, *Icarus*, **192**(1) (2007), pp. 223–237.
- 20) Hanuš, J., Durech, J., Brož, M., Warner, B. D., Pilcher, F., Stephens, R., Oey, J., Bernasconi, L., Casulli, S., Behrend, R., Polishook, D., Herych, T., Lehký, M., Yoshida, F. and Ito, T.: A Study of Asteroid Pole-Latitude Distribution Based on an Extended Set of Shape

Models Derived by the Lightcurve Inversion Method, *Astronomy & Astrophysics*, **530(A134)** (2011), pp. 1–16.

- 21) Rios-Reyes, L. and Scheeres, D. J.: Generalized Model for Solar Sails, *Journal of Spacecraft and Rockets*, **42(1)** (2005), pp. 182–185.
- 22) Rios-Reyes, L. and Scheeres, D. J.: Solar-Sail Navigation: Estimation of Force, Moments, and Optical Parameters, *Journal of Guidance, Control, and Dynamics*, **30(3)** (2007), pp. 660–668.
- 23) McInnes, C. R.: *Solar Sailing: Technology, Dynamics and Mission Applications, First edition*, Springer Praxis, Chichester, UK, 1999.
- 24) Scheeres, D. J.: *Orbital Motion in Strongly Perturbed Environments, First edition*, Springer Praxis, Chichester, UK, 2012.
- 25) Jordan, D. W. and Smith, P.: *Nonlinear Ordinary Differential Equations: An introduction for Scientists and Engineers, Fourth edition*, Oxford University Press, New York, 2007.
- 26) Scheeres, D. J. and Marzari, F.: Spacecraft Dynamics in the Vicinity of a Comet, *Journal of the Astronautical Sciences*, **50(1)** (2002), pp. 35–52.
- 27) Chujo, T., Shirasawa, Y., Mori, O. and Kawaguchi, J.: Study and Development of Advanced Reflectivity Control Device for Spin Rate Control, *30th International Symposium on Space Technology and Science*, paper 2015-d-24.